

A Rapid, Label-free and Impedimetric DNA Sensor Based on PNA-modified Nanoporous Gold Electrode

Wenyan Tao^{1,2}, Peng Lin^{1,*}, Hong Liu¹, Shanming Ke¹ and Xierong Zeng¹

¹Shenzhen Key Laboratory of Special Functional Materials & Shenzhen Engineering Laboratory for Advance Technology of Ceramics, College of Materials Science and Engineering, Shenzhen University, Shenzhen, China

²Key Laboratory of Optoelectronic Devices and Systems of Ministry of Education and Guangdong Province, College of Optoelectronic Engineering, Shenzhen University, Shenzhen, China

*E-mail: lin.peng@szu.edu.cn

Received: 21 July 2017 / Accepted: 1 September 2017 / Published: 12 October 2017

A gold nanoparticle film was successfully prepared on highly ordered and porous anodic aluminum oxide substrate through thermal evaporation deposition technique. As-fabricated nanoporous gold electrode modified by thiol-derivative peptide nucleic acid (PNA) was applied for impedimetric DNA sensing. *In-situ* kinetic analysis of PNA/DNA hybridization process was realized by electrochemical impedance spectroscopy (EIS) method. Considering the special structure of nanoporous gold electrode, a new equivalent circuit model was proposed for EIS data fitting. The sensitivity of PNA-modified nanoporous gold electrode is 0.4 $\Omega/\text{cm}^2 \cdot \text{nM}$. Meanwhile, complementary DNA target could be detected at concentration as low as 10 nM, which indicating that a methodology for rapid, sensitive and label-free detection of DNA has been set-up based on nanoporous gold electrode.

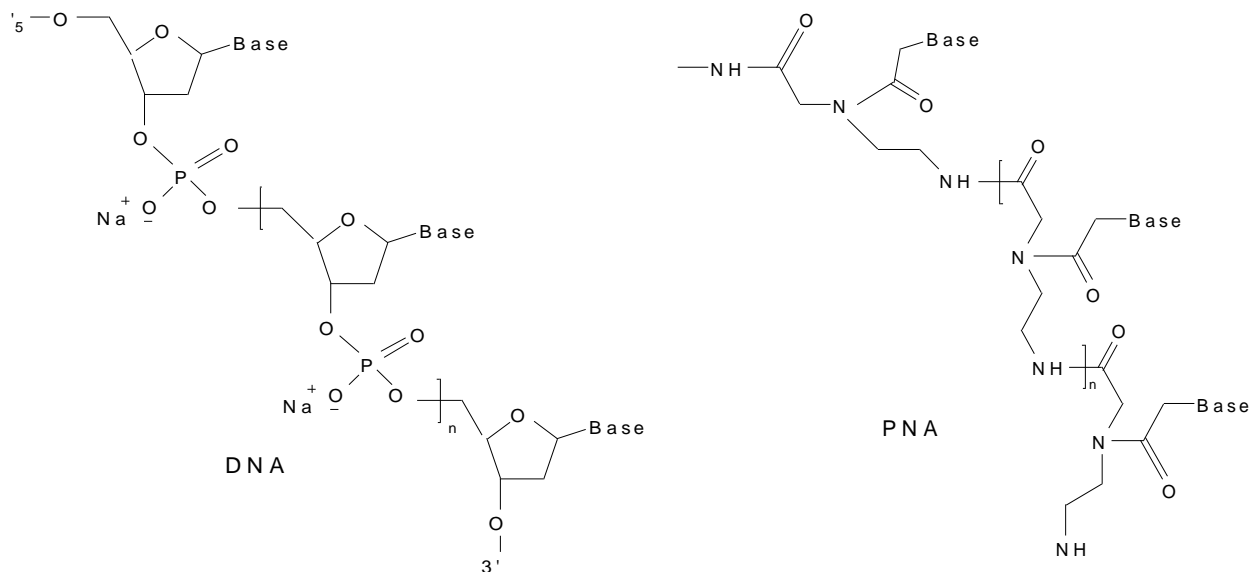
Keywords: anodic aluminum oxide; nanoporous gold electrode; peptide nucleic acid; DNA sensing

1. INTRODUCTION

DNA hybridization process is significant to chip-based characterization of gene expression pattern and pathogens detection. Commonly, optical method was used to monitor DNA hybridization process or recognize DNA point mutation [1-3]. In order to address the sensitivity issues, the polymerase chain reaction has been integrated into optical sensors to amplify the target DNA [4], which is tedious and time-consuming. Therefore, rapid and label-free DNA sensors with many strategies including electronic [5], colorimetric [6], and electrochemical [7] sensing mechanisms have been developed. These methods avoid using the fluorescent labels, which is more attractive to the user.

For example, a label-free colorimetric method was presented for simple and convenient assay of DNA methylation using unmodified Au nanorods with enzyme-linkage reaction [6]. In this method, DNA methylation and MTase activity can be readily monitored by the color change of Au nanorods.

Peptide nucleic acid (PNA) is an achiral and uncharged DNA mimic where the sugar-phosphate backbone has been replaced with a peptide like *N*-(2-aminoethyl) glycine polyamide structure, to which the nucleobases are connected by methylenecarbonyl linkages (Scheme 1).



Scheme 1. The structure skeleton of DNA and PNA.

PNA has been paid many attentions in electrochemical [8-10] and fluorescent method for DNA sensing [11]. PNA probe possesses two main advantages over DNA probe for hybridization: firstly, no electrostatic repulsion between PNA and negatively charged DNA, which make PNA can be highly hybridized with DNA. Secondly, PNA possesses excellent stability. PNA oligomers are neither degraded by nucleases nor proteases. Finally, no enantiomeric purity issue in PNA solution occurs due to achiral structure of PNA. Specially, facilitated by the difference in surface charge between DNA probe and duplex DNA chains, electrochemical impedance spectroscopy (EIS) method has been used in DNA sensing on the gold and boron-doped diamond electrode [12,13]. The principle of impedimetric DNA sensing is based on the formation of PNA/DNA duplex at the sensing surface. Then the negatively charged interface repels the negatively charged redox indicator, which leading to an increase in charge transfer resistance or other electric elements related to the PNA/DNA duplex. Therefore, these electric elements will increase with the increase of DNA concentration.

On the other hand, porous anodized aluminum oxide (AAO) substrate is a type of feasible, low-cost, versatile inorganic materials for wide applications in filtration [14], protein separation [15], catalysis [16], biosensing [17] and nanofabrication [18]. AAO substrates consist of highly-ordered and uniform nanopores with large depth/width ratio (>1000) [19, 20]. The pore diameter and depth can be adjusted by the anodization conditions such as acid types, pH value, temperature and anodizing time etc. [21-24]. AAO and polymeric membranes are two typical classes of templates employed for the

nano-structural films fabrication [25, 26]. AAO provides a rough surface with large surface area for supporting metal nanoparticles and formed a conductive nano-structural network which facilitates measurement of electrical property changes. Until now, there is few work based on AAO template for DNA sensing. A microfluidic-channel based electrochemical DNA biosensor was constructed by using AAO substrates as the designing templates [27]. The DNA biosensor provides 10^{-19} M sensitivity for detecting target DNA, which through hybridizing with flow-forced filtration of target DNA solution. Such high sensitivity is attributed to the well-defined fluidic channel structure that gives high surface area for probe DNA immobilization and enables target DNA solutions to pass through its fluidic channels for rapid and efficient hybridization. However, the fabrication of microfluidic channel is complex and time-consuming.

In this work, a type of nanoporous gold electrode fabricated on AAO substrate was used as a novel electrode for DNA sensing. Using PNA as probe, a rapid, label-free and impedimetric DNA biosensor was constructed on the nanoporous gold electrode. A new equivalent circuit model was proposed and applied in data analysis.

2. EXPERIMENTAL

2.1. Chemicals and materials

Synthesis of PNA probe is according to the following rules: 1) the base number of PNA probe is limit in the range of 10 to 18 for good affinity; 2) high purine content will cause aggregation and low solubility. It is suggested that purine content not exceeds 60%. Thiolated PNA probe was synthesized from ZIYU Biotech Co. Ltd (Shanghai, China), and target DNA were purchased from Shanghai Sangon Ltd (Shanghai, China), shown in Table 1.

Table 1. The sequences of PNA probe and DNA targets

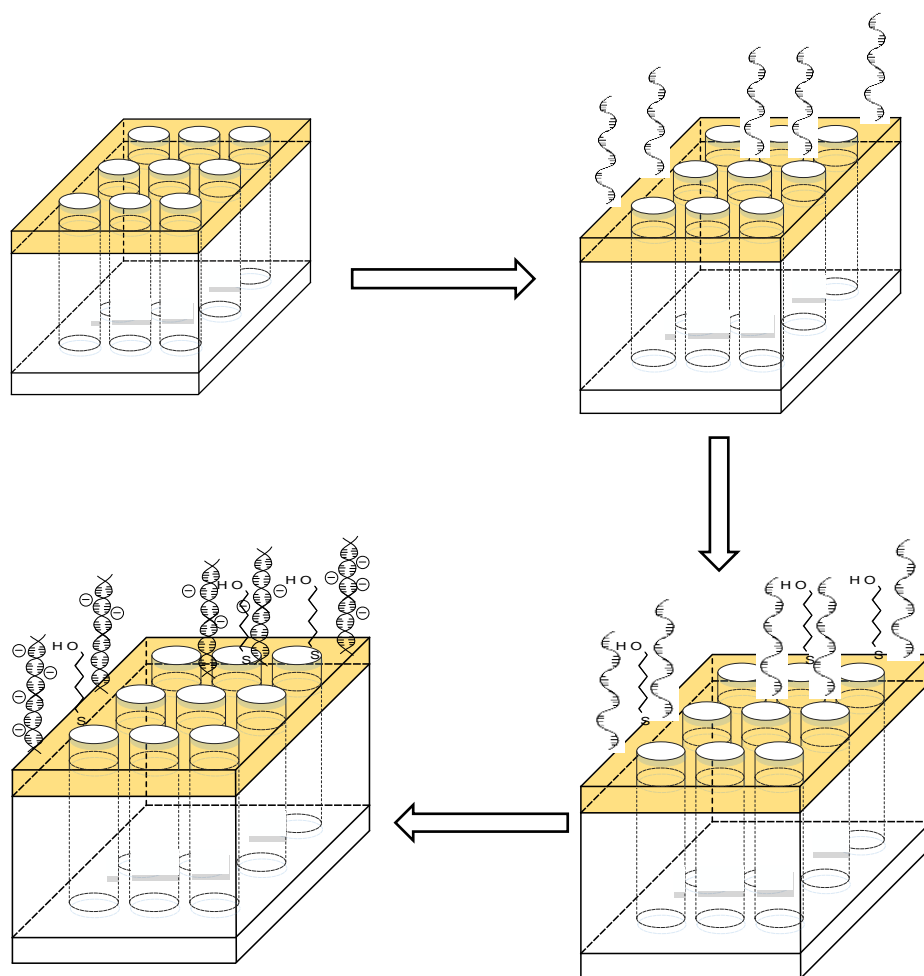
Name	Sequences
PNA probe	Cys-OO-TACTAAGTCT-CONH ₂
Complementary DNA target (C-DNA)	5'-ATGATTCAGA-3'
Completely mismatched DNA target	5'-CGTTAAAGTC-3'

Cys-OO-:

Mercaptohexanol (MCH), $K_3Fe(CN)_6$ and $K_4(FeCN)_6$ were of analytical grade reagents. 50 mM Tris-HCl buffer was used to store and transport DNA (pH 7.4), and 10 mM phosphate-buffered saline (PBS, pH 7.0) was used as an aqueous electrolyte for testing. Porous anodic aluminum oxide (AAO) membrane with average pore size of 200 nm was purchased from Whatman (Whatman International Ltd.). The diameter of circle-shaped AAO substrate is 13 mm and its thickness is 60 μ m. Water used

for sample preparation was deionized on a micro-pure water purification system with resistivity of 18.2 M Ω ·cm.

2.2 Preparation and modification of nanoporous gold electrode



Scheme 2. Schematic illustrations of PNA immobilization and PNA/DNA hybridization process on nanoporous gold electrode.

A thin gold nanoparticle film was prepared on AAO substrate by thermal evaporation deposition technique, named as nanoporous gold electrode in this work. Before film deposition, the AAO substrate were rinsed with ethanol and distilled water alternatively, dried in ambient air, and then fixed on a silicon plate. Then the AAO substrate was moved to a chamber of Nexdep Thin film 400 deposition system. The deposition rate was set at 0.1 Å/s in the vacuum of approximately 1×10^{-7} Torr. After desired thickness of ~40 nm was obtained, as fabricated nanoporous gold electrode was kept in a vacuum container prior to use.

The modification process of nanoporous gold electrode is as follows: immersed the electrode into 10 μM thiolated PNA solution for 12 hrs, followed by rinsing with PBS and water three times to remove physically absorbed PNA molecule. Finally, the electrode was further treated with 1 mM MCH solution for 2 hrs to block the unoccupied site, rinsing with PBS and water three times prior to detection. The detail PNA modification and PNA/DNA hybridization process was shown in Scheme 2.

2.3 Measurement

Cyclic voltammetry and electrochemical impedance spectroscopy were recorded on CHI 660E working station (CHI Instruments, Inc. USA). Three-electrode system was employed with saturated calomel electrode as reference electrode, a platinum plate as counter electrode, and PNA-modified or PNA/DNA-modified nanoporous gold electrode (diameter, 3 mm) as working electrode. The amplitude of modulation potential is 5 mV, and the frequency range is from 100 kHz to 1 mHz. Data analysis was performed with ZSimpWin 3.21 software using the proposed equivalent circuit. Meanwhile, scanning electron micrographs (SEM) were obtained on a JSF-6700 field emission scanning electron microscope at an operation potential of 10 kV. At least five nanoporous gold electrodes were measured at each time and the mean value was utilized. All measurements were carried out at room temperature (25 ± 2 °C).

3. RESULT AND DISCUSSION

3.1. SEM characterization

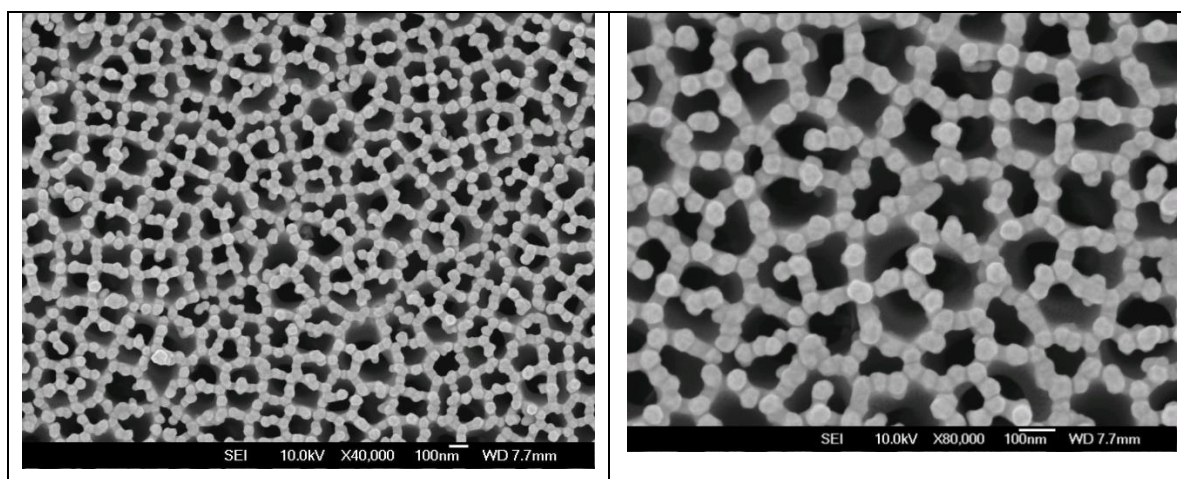


Figure 1. Field-emission SEM images of nanoporous gold electrode. The scale bar is 100 nm. The magnification is $\times 40000$ and $\times 80000$, respectively.

As shown in Figure 1, gold nanoparticles and holes are linked with each other regularly in the nanoporous gold electrode. Several structural features emerged from the micrographs. First, gold film was deposited on AAO substrates mainly by surrounding the nanopores. Second, the gold film mainly

consists of nanoparticles in good homogeneity. It suggests that the deposited gold nanoparticles are in good crystalline structure, similar with that in the previous work [28]. Meanwhile, calculated from the images, the average diameter of gold nanoparticles and the “surface” filling factor are around 55.1 ± 0.7 nm and 0.62 ± 0.06 , respectively. So, gold nanoparticles linked with each other along the AAO substrate frames and formed a compact structure. The special structure suggests that the physicochemical properties of nanoporous gold electrode would be affected not only by that of individual particles but also by their ring-shaped aggregates [28]. Compared to the conventional flat gold electrode, the individual particles and their linear and ring shaped aggregates make the nanoporous gold electrode possess larger active electrochemical area and higher conductivity, which facilitate the electron transfer and result in higher sensitivity for DNA sensing.

3.2. In-situ monitoring PNA/DNA hybridization

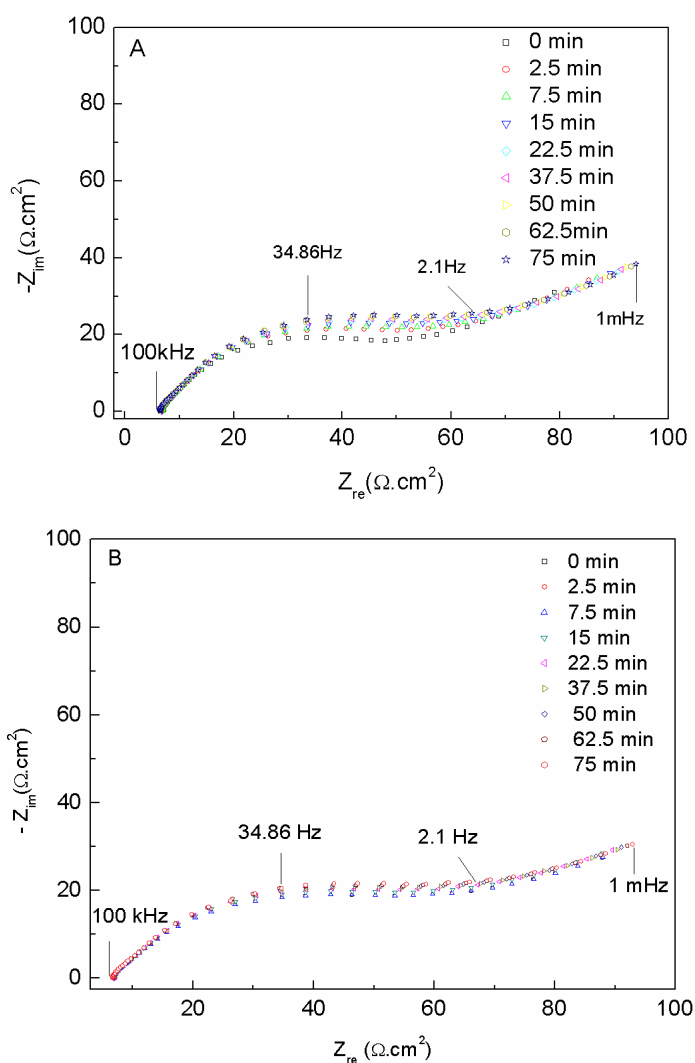


Figure 2. Nyquist plots of PNA-modified nanoporous gold electrode in the presence of 500 nM complementary DNA target (A) and completely mismatched DNA target (B) with different hybridization time. Buffer: 50 mM PBS containing 0.5 M NaCl, pH 7.4. Redox probe: 1mM/1mM $\text{Fe}(\text{CN})_6^{3-/4-}$.

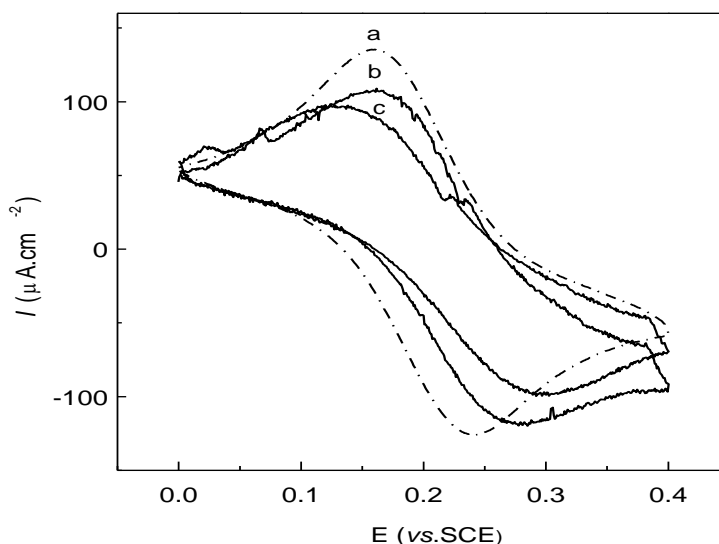


Figure 3. Cyclic Voltammograms of 1 mM $\text{Fe}(\text{CN})_6^{3-/4-}$ on bare electrode (a), PNA-modified (b) and PNA/DNA-modified (c) nanoporous gold electrodes. 500 nM complementary DNA target was used for hybridization. Scan rate: 10 mV/s.

EIS is a simple and convenient method for *in-situ* kinetic study of PNA/DNA hybridization. Figure 2A shows the faradaic impedance spectra of PNA-modified nanoporous gold electrode in the presence of 500 nM complementary DNA target with different hybridization times. Since PNA is neutral and DNA possesses some negative charges (shown in Scheme 1), the electrode surface was turned from neutral to negative after hybridization. Obviously, the electron-transfer resistance (R_{ct}), which is correlated to the diameter of Nyquist plot semicircle, increased gradually with increasing hybridization time.

It is consistent with the electrostatic repulsion of $\text{Fe}(\text{CN})_6^{3-/4-}$ from the electrode interface by formation of negative charged PNA/DNA duplex, thereby introducing a barrier for interfacial electron transfer. R_{ct} reached a plateau value after 75 minutes, indicating that the PNA/DNA hybridization reaction reached equilibrium. Impedance data for non-complementary DNA targets were shown in Figure 2B as control. No obvious change in semicircle was observed, indicating no hybridization reaction occurred for non-complementary DNA targets.

Meanwhile, cyclic voltammetry was used to characterize the PNA/DNA hybridization. As shown in Figure 3, peak currents for the three nanoporous gold electrodes are in the following order: bare > PNA-modified > PNA/DNA-modified. It means that PNA was successfully assembled on the bare electrode, which hindered redox probe diffusing to electrode surface. For PNA/DNA-modified electrode, the charge repulsion between negative DNA and negative redox probe resulted in the further decrease in peak current. It is consistent with the increase of the electron-transfer resistance in EIS results.

3.3. New equivalent circuit model

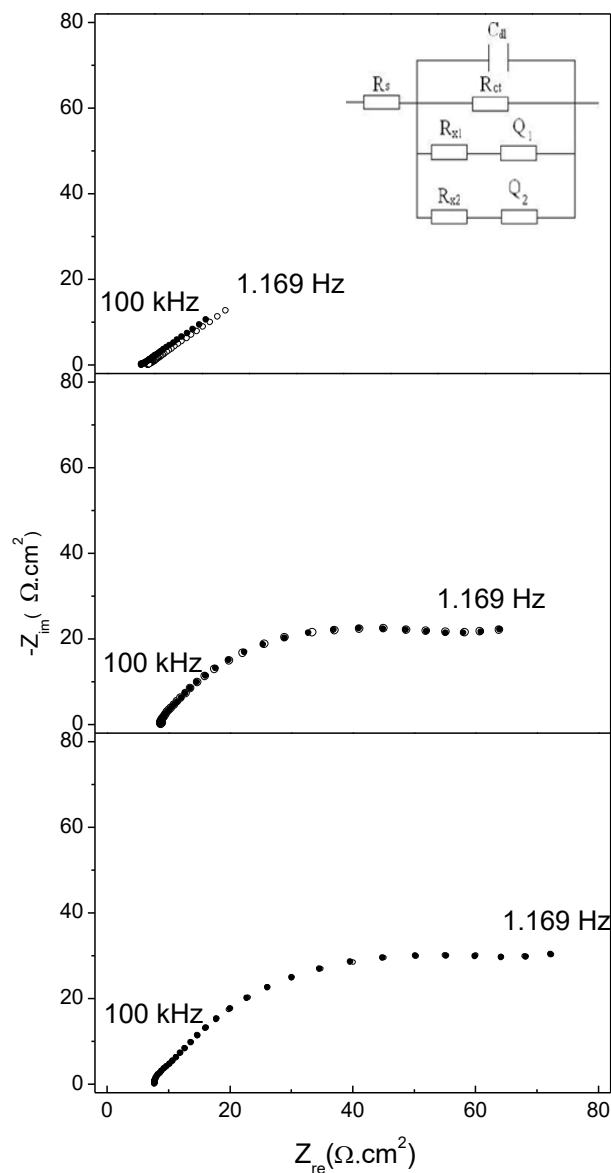


Figure 4. Representative Nyquist plots of bare (top), PNA-modified (middle) and PNA/DNA-modified (bottom) nanoporous gold electrodes in 50 mM PBS buffer containing 1mM/1mM $\text{Fe}(\text{CN})_6^{3-/4-}$. Measured data were shown as open circle and fitted data shown as solid ones. A new equivalent circuit model was shown in the inset figure. R_s : solution resistance; C_{dl} : double layer capacitance; R_{ct} : charge-transfer resistance; R_{x1} : resistance through the PNA or PNA/DNA films; R_{x2} : pinhole/defect resistance; Q_1 , Q_2 : constant phase element.

Figure 4 demonstrated Nyquist plots of bare, PNA-modified and PNA/DNA-modified nanoporous gold electrode in the buffer containing $\text{Fe}(\text{CN})_6^{3-/4-}$ redox probe. Since Warburg impedance is absence in the new equivalent model, diffusion of the redox probe to PNA or PNA/DNA films could be ignored in this work. Therefore, data within in the high frequency range (100 kHz to 1.169 Hz)

corresponding to the electron-transfer-limited process was collected for data analysis. Data at lower frequency representing the diffusion-limited process is not shown in this work.

Table 2. Comparison of the fitting data analyzed by the new equivalent circuit model for PNA-modified and PNA/DNA-modified nanoporous gold electrodes

Parameter	PNA-modified	PNA/DNA-modified	Difference value
$R_s(\Omega \cdot \text{cm}^2)$	7.05	6.38	-0.67
$C_{dl}(\text{F}/\text{cm}^2)$	2.64E-5	2.46E-5	-1.8E-6
$R_{ct}(\Omega \cdot \text{cm}^2)$	84.57	103.84	19.27
$Q_1-Y_0(\text{F}/\text{cm}^2)$	4.68E-4	2.28E-4	-2.4e-4
Q_1-n	0.89	0.99	0.1
$R_{x1}(\Omega \cdot \text{cm}^2)$	111.45	179.56	68.11
$Q_2-Y_0(\text{F}/\text{cm}^2)$	1.88E-4	2.12E-4	2.4e-5
Q_2-n	0.77	0.78	0.01
$R_{x2}(\Omega \cdot \text{cm}^2)$	5.74	6.4	0.66

Complementary DNA target concentration: 200 nM

Fitted data was shown as solid line in Figure 4 and detail results were listed in Table 2. Considering the special structure of nanoporous gold electrode, reported Randles model for DNA/DNA duplex was not applicable [29, 30]. A new equivalent circuit model with paralleled (RQ) component was proposed in this work, shown in the inset figure of Figure 4. Electronic elements in the new equivalent circuit are described below. Solution resistance (R_s), is related to the resistance between reference electrode and working electrode. To minimize variations in R_s , the distance between the two electrodes was kept constant in all the measurements. The values of R_s for PNA and PNA/DNA films are almost similar, which range from 6 to 7 $\Omega \cdot \text{cm}^2$. C_{dl} accounts for the double layer capacitance of the film on nanoporous gold electrode. The value for PNA/DNA film is a little smaller than that for PNA film. It may result from the increase in film thickness and charge repulsion force after PNA hybridized with DNA. R_{x1} is related to resistance through PNA or PNA/DNA film; R_{x2} is related to the pinhole/defect resistance of nanoporous gold electrode. The combination of R_{x1} and constant phase element (Q_1) accounts for resistance through PNA or PNA/DNA film. Q_1 acts as a nonlinear capacitor related to film in homogeneity and electrode surface [31]. Values for Q_1 range from 0.2 to 0.5 $\text{mF} \cdot \text{cm}^{-2}$, with the exponential modifier factor of 0.9. The value for R_{x1} on PNA film is totally different from that on PNA/DNA film. The other pair of combination of R_{x2} and the constant phase element (Q_2) accounts for the pinhole/defect resistance of nanoporous gold electrode. Values of R_{x2} for the two films are almost the same, 5.74 $\Omega \cdot \text{cm}^2$ for PNA and 6.40 $\Omega \cdot \text{cm}^2$ for PNA/DNA film. Values for Q_2 vary in a small range of $\pm 0.024 \text{ mF} \cdot \text{cm}^{-2}$. The value for R_{ct} (2.65 $\Omega \cdot \text{cm}^2$) on flat gold electrode is near to that for R_{x2} on PNA-modified nanoporous gold electrode (5.74 $\Omega \cdot \text{cm}^2$), indicating that resistance from defect sites in the gold nanoparticle film is small, and pores in the electrode do not effect DNA detection.

3.4 DNA Sensing

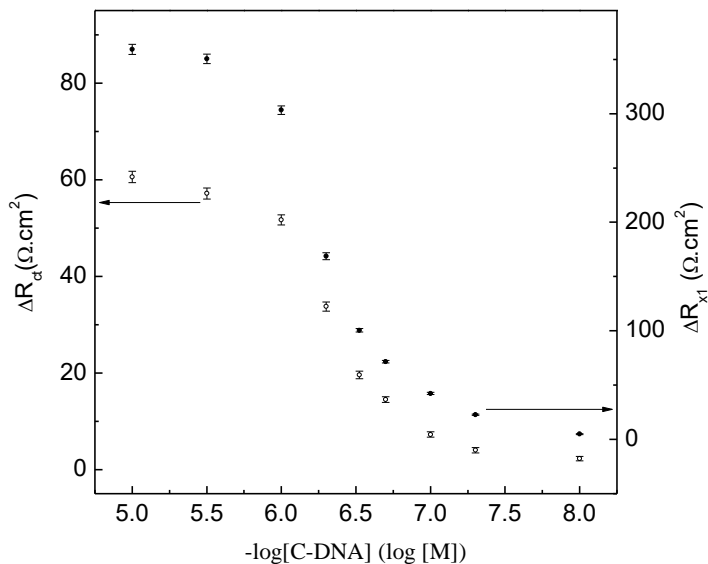


Figure 5. The Relationship between resistances and complementary DNA target concentration.

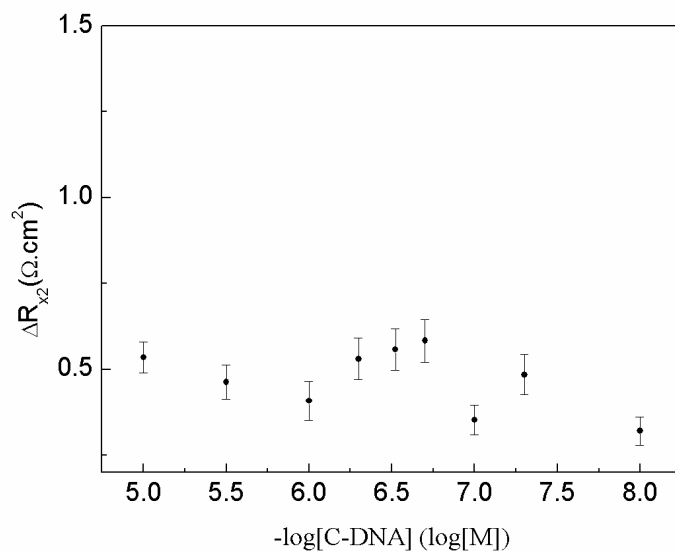


Figure 6. The Relationship between ΔR_{x2} and complementary DNA target concentration.

Generally, the charge-transfer resistance, R_{ct} , is the key parameter, which varying with DNA target concentration. Meanwhile, in the new equivalent model, R_{x1} increases with the increase of DNA concentration. Therefore, both R_{ct} and R_{x1} were plotted with DNA concentration, shown in Figure 5. Meanwhile, the relationship between R_{x2} and DNA concentration was plotted as Figure 6.

The dependence of R_{ct} or R_{x1} on DNA concentration follows a classical binding curve. Obviously, the increase in R_{x1} is much larger than that in R_{ct} . However, there is no response of R_{x2} to

DNA concentration. The reason is that R_{x2} is only related to the pinhole/defect resistance in the electrode. No defect site formed during PNA/DNA hybridization process. The detectable concentration of complementary DNA is 10 nM using R_{x1} as response factor. The sensitivity for PNA-modified electrode is $0.4 \Omega / \text{cm}^2 \cdot \text{nM}$, which is higher than that reported in the literature [32].

The DNA sensing performance in this work was compared with those in recent reports using other techniques. Results were listed in **Table 3**. Obviously, flurometric method is more sensitive for DNA sensing [2, 33]. However, output signal is not so stable because the fluorescent marker is easier to quench in detection process. Meanwhile, flurometric method is involved fluorescent marker-labeling, which is tedious and time-consuming. Lower detectable DNA concentrations were obtained in other works utilizing electrochemical techniques such as CV, ADPV and DPV [34, 35], in which indicator and electrode pretreatment must be used for signal acquiring process. It should be noted that the detection limit was measured to 10 nM using R_{x1} as response factor in this work. The value is lower than that reported on boron-doped diamond (BDD) electrode using the EIS technique [36], which involved BDD electrode modification process of polyaniline/polyacrylate layer. The value (10 nM) is same with that on similar working electrode-nanoporous gold electrode reported in reference [37]. In that report, SWV technique was adopted, in which the indicator of methylene blue had to be used. In this work, no label and no indicator are in need. Therefore, a methodology for rapid, sensitive and label-free detection of DNA has been set-up based on nanoporous gold electrode in this work. Additionally, it should be noted that the sensor discussed in this work was not optimized for lower detection limit. It can be significantly improved by reducing electrochemical cell volume (*e.g.*, microfluidics) and electrode size to optimize target-to-electrode transport and reaction rates.

Table 3. Comparison of DNA sensing in some reports with that in this work

Sensing Substrate	Label/Indicator	Probe	Modified layer/ Pretreatment	Detection Method	Stability	LOD (nM)	Ref.
NA	Ce(QS) ₂ Cl	DNA	None	Flurometric	Poor	0.07	[2]
Etched optical fiber	bi-p,p'-4-Hydroxyphenylacetic acid	DNA	Streptavidin labeled horseradish peroxidase	Flurometric	Poor	0.001	[33]
CPE	Methylene blue	DNA	Zirconia	CV/DPV	Common	0.2	[34]
PGE	None	DNA	Pretreatment in acetate buffer	ADPV	Common	0.069	[35]
BBDE	None	DNA	Polyaniline/Polyacrylate	EIS	Good	20	[36]
NGE	Methylene blue	DNA	None	SWV	Good	10	[37]
NGE	None	PNA	None	EIS	Excellent	10	TW

ADPV: anodic differential pulse voltammetry; DPV: differential pulse voltammetry; SWV: square wave voltammetry; CV: cyclic voltammetry; CPE: Carbon paste electrode; BBDE: Boron-doped diamond electrode; PGE: Pencil graphite Electrode; NGE: Nanoporous gold electrode; TW: this work; NA: not applicable.

4. CONCLUSION

In this work, a methodology for rapid, sensitive and label-free detection of DNA has been set-up based on nanoporous gold electrode. A new equivalent circuit model with two paralleled (RQ)

component was proposed for nanoporous gold electrode. R_{x1} is related to resistance through PNA or PNA/DNA film; R_{x2} is related to the pinhole/defect resistance of nanoporous gold electrode. It is worth to be noticed that R_{x1} increased faster than that in charge transfer resistance with the increase of DNA concentration. Therefore, using R_{x1} as the response factor, sensitivity of $0.4 \Omega/\text{cm}^2 \cdot \text{nM}$ and detectable concentration of complementary DNA 10 nM were obtained on the nanoporous gold electrode.

ACKNOWLEDGEMENT

This work was supported by the National Natural Science Foundations of China (No. 21405106), the Foundation for Distinguished Young Talents in Higher Education of Guangdong, China (No. 2014KQNCX130), the Natural Science Foundation of Shenzhen University (No. 827-000022), and the Research and Development Foundation of Science and Technology of Shenzhen (Nos. JCYJ20150324141711592 and JCYJ20170302145633009).

References

1. R. M. Hawk, M. V. Chistiakova and A. M. Armani, *Opt. Lett.*, 38 (2013) 4690.
2. M. Shamsipur, Z. Memari, M. R. Ganjali, P. Norouzi and F. Faridbod, *J. Pharm. Biomed. Anal.*, 118 (2016) 356.
3. Y. Fan, K. Hotta, A. Yamaguchi, Y. Ding and Y. He, *Appl. Phys. Lett.*, 105 (2014) 031103.
4. M. J. Walker and R. Rapley, *Molecular Biology and biotechnology*, The Royal Society of Chemistry. Thomas Graham House, 2000, Cambridge, U.K.
5. M. Berggren and A. Richter-Dahlfors, *Adv. Mater.*, 19 (2007) 3201.
6. X. J. Zheng, J. D. Qiu, L. Zhang, Z. X. Wang and R. P. Liang, *Chem. Commun.*, 49 (2013) 3546.
7. A. S. Patterson, K. Hsieh, H. T. Soh and K. W. Plaxco, *Trends Biotechnol.*, 31 (2013) 704.
8. H. Gaiji, P. Jolly, S. Ustuner, S. Goggins and M. Abderrabba, *Electroanalysis*, 28 (2016) 1.
9. J. D. Besant, I. B. Burgess, W. H. Liu, E. H. Sargent and S. O. Kelley, *Nat. Commun.*, 22 (2015) 6978.
10. S. Kelley, R. Gasparac, M. Lapierre-devlin and B. Taft, *Electrocatalytic nucleic acid hybridization detection*. US20040913925 [P] 2004-08-06.
11. P. M. Sabale, J. T. George and S. G. Srivatsan, *Nanoscale*, 6 (2014) 10460.
12. Y. Wang, C.J. Li, X. H. Li, Y. F. Li and H. Kraatz, *Anal. Chem.*, 80 (2008) 2255.
13. J. Weng, J. Zhang, H. Li, L. Sun, C. Lin and Q. Zhang, *Anal. Chem.*, 80 (2008) 7075.
14. Y. Park, S. Kim, I. H. Jang, Y. S. Nam, H. Hong, D. Choi and W. G. Lee, *Analytst*, 1 (2016) 451.
15. W. Shi, Y. Q. Shen, D. T. Ge, M.Q. Xue, H. H. Cao, S. Q. Huang, J. X. Wang, G. L. Zhang, and F. B. Zhang, *J. Membrane Sci.*, 325 (2008) 801.
16. F. Liu, J. Y. Lee and W. J. Zhou, *Small*, 2 (2006) 121.
17. A. Santos, T. Kumeria and D. Losic, *Trends Anal. Chem.*, 44 (2013) 25.
18. P. Ciambelli, L. Arurault, M. Sarno, S. Fontorbes, C. Leone, L. Datas, D. Sannino, P. Lenormand and S. Le Blond Du Plouy, *Nanotech.*, 22 (2011) 265613.
19. F. Li, L. Zhang and R. Metzger, *Chem. Mater.*, 10 (1998) 2470.
20. C. C. Lu, Y.S. Huang, J. W. Huang, C. K. Chang and S. P. Wu, *Sensors*, 10 (2010) 670.
21. H. Masuda and K. Fukuda, *Science*, 268 (1995) 1466.
22. H. Masuda and M. Satoh, *Jpn. J. Appl. Phys.*, 35 (1996) L126.
23. H. Masuda, K. Yada and A. Osaka, *Jpn. J. Appl. Phys.*, 37 (1998) L1340.
24. K. Schwirn, W. Lee, R. Hillebrand, M. Steinhart and K. Nielsch, *ACS Nano*, 2 (2008) 302.

25. Y. Piao, H. Lim, J. Y. Chang, W. Y. Lee and H. Kim, *Electrochim. Acta*, 50 (2005) 2997.
26. H. Su, Y. Li, X.Y. Li and K. S. Wong, *Opt. Express*, 17 (2009) 22223.
27. Y. J. Kim, J. E. Jones, H. Li, H. Yampara-Iquise, G. L. Zheng, C. A. Carson, M. Cooperstock, M. Sherman and Q. S. Yu, *J. Electroanal. Chem.*, 702 (2013) 72.
28. Y. S. Li, H. M. Su, K. S. Wong and X. Y. Li, *J. Phys. Chem. C.*, 114 (2010) 10463.
29. Y. T. Long, C. Z. Li, H. B. Kraatz and J. S. Lee, *Biophys. J.*, 84 (2003) 3218.
30. X. Li, J. S. Lee and H. B. Kraatz, *Anal. Chem.*, 78 (2006) 6096.
31. M. Dijkstra, B. A. Boukamp, B. Kamp and W. P. Bennekoum, *Langmuir*, 18 (2002) 3105.
32. A. Kukol, P. Li, P. Estrela, P. K.o-Ferrigno and O. Migliorato, *Anal. Biochem.*, 374 (2008) 143.
33. S.Y. Niu, Q.Y. Li, R. Ren and S.S. Zhang, *Biosens. Bioelectron.*, 24 (2009) 2943.
34. S.H. Zuo, L. F. Zhang, H. H. Yuan, M. B. Lan, G. A. Lawrance and G. Wei, *Bioelectrochemistry*, 74 (2009) 223.
35. M. H. Pournaghi-Azar, E. Alipour, S. Zununi, H. Froohandeh and M. S. Hejazi, *Biosens. Bioelectron.*, 24 (2008) 524.
36. H.R. Gu, X.D. Su and K. P. Loh, *J. Phys. Chem. B*, 109 (2005) 13611.
37. P. Daggumati, Z. Matharu and E. Seker, *Anal. Chem.*, 87 (2015) 8149.

© 2017 The Authors. Published by ESG (www.electrochemsci.org). This article is an open access article distributed under the terms and conditions of the Creative Commons Attribution license (<http://creativecommons.org/licenses/by/4.0/>).